THE JOURNAL OF PHYSICAL CHEMISTRY C

Article

pubs.acs.org/JPCC

Origin of the $\pi-\pi$ Spacing Change upon Doping of Semiconducting Polymers

Wenlan Liu,[†,‡,§,¶] Lars Müller,[‡,∥,⊥,¶] Shuangying Ma,[‡,§] Stephen Barlow,[#] Seth R. Marder,[#] Wolfgang Kowalsky,[‡,∥] Andreas Köhn,[*,‡,§] and Robert Lovrincic[*,‡,∥]

[†]Chongqing Key Laboratory of Green Synthesis and Applications & College of Chemistry, Chongqing Normal University, Chongqing 400047, China

[‡]InnovationLab, Heidelberg 69115, Germany

[§]Institute for Theoretical Chemistry, University of Stuttgart, Stuttgart 70174, Germany

[∥]Institute for High-Frequency Technology, TU Braunschweig, Braunschweig 38106, Germany

[⊥]Kirchhoff Institute for Physics, Heidelberg University, Heidelberg 69117, Germany

[#]Center for Organic Photonics and Electronics and School of Chemistry and Biochemistry, Georgia Institute of Technology, Atlanta, Georgia 30332-0400, United States

Supporting Information

ABSTRACT: Although there is an agreement about the local structural order of semiconducting polymers such as poly(3-hexylthiophene) (P3HT), there is still a debate over the impact of molecular doping. One prevalent interpretation is that dopant molecules intercalate in the $\pi-\pi$ stacking of crystallites; however, this idea has recently been challenged. We present here electron diffraction measurements of P3HT doped with the two dopants 2,3,5,6-tetrafluoro-7,7,8,8-tetracyanoquinodimethane (F_4TCNQ) and molybdenum tris[1-(methoxycarbonyl)-2-(trifluoromethyl)-ethane-1,2-dithiolene] (Mo(tfd-CO_2Me)$_3$), which have considerably different sizes and shapes, processed by different doping techniques. We observe a reduction in the $\pi-\pi$ spacing of P3HT upon doping with both dopant molecules and doping techniques. These data are not consistent with both of the dopants intercalating in the $\pi-\pi$ stacks and an alternative explanation is, therefore, required to explain these results. Density functional theory calculations for P3HT model oligomers suggest that the polaron delocalizes between adjacent chains and thus leads to attractive forces that reduce the $\pi-\pi$ spacing, without the physical presence of any dopant molecules. Our study emphasizes that not only geometric effects induced by dopant molecules lead to the observed reduction of $\pi-\pi$ spacing, but the charging itself.

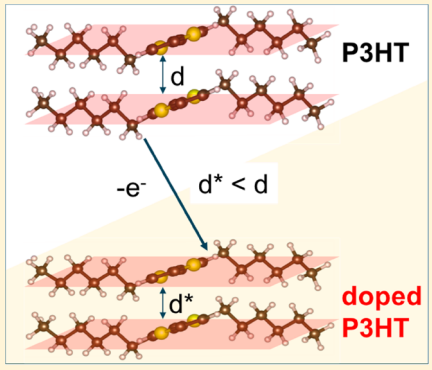

1. INTRODUCTION

The performance of organic electronic devices such as field-effect transistors or solar cells depends on the charge transport within the organic materials.[1] In conjugated polymers, electrical conductivity is known to be strongly influenced by the local structural order and can be furthermore tuned in a broad range with molecular doping.[2] The complex polymer−dopant interactions and their effect on charge transport are an area of active research. For instance, recent studies found a decrease of the $\pi-\pi$ interchain distance in polymers upon doping.[3−9] As we outline below, several, sometimes contradictory, explanations for this decrease have been proposed and a generally accepted understanding of the underlying mechanism is lacking.

The most investigated semiconducting polymer poly(3-hexylthiophene) (P3HT) is semicrystalline, with ∼20 nm crystallites embedded in an amorphous matrix. These crystallites show distinct lattice spacings: the lamellar stacking in the [100]-direction with a spacing of 1.68 nm in the direction of alkyl side chains and the stacking in the [010]-direction, usually named $\pi-\pi$ spacing, with a distance of 0.38 nm. Depending on the angle between side chains and backbone, the spacing in the [010]-direction fully or partly corresponds to the spacing orthogonal to and between the backbones.[9−11] Despite numerous publications that specifically address the structural order and its emergence in the case of molecular dopants present in the polymer matrix, the exact local structure and its formation are still under discussion.[6,9,12−14]

Among the first investigations on this topic was a study on the host:dopant model system P3HT:2,3,5,6-tetrafluoro-7,7,8,8-tetracyanoquinodimethane (F_4TCNQ) in which doping was achieved by mixing the dopant and host in a solution prior to spin coating. After film formation, X-ray diffraction measurements on F_4TCNQ-doped P3HT revealed two distinct diffraction peaks around the spacings expected for the $\pi-\pi$

Received: November 7, 2018
Revised: November 16, 2018
Published: November 16, 2018

DOI: 10.1021/acs.jpcc.8b10845
J. Phys. Chem. C XXXX, XXX, XXX−XXX

interchain distance. One of the spacings was smaller compared to the $\pi-\pi$ stacking distance of two polymer backbones, whereas the second was slightly larger. Although the authors acknowledged that the amount of structural information that could be extracted from the diffraction data was limited, they suggested that cocrystals were formed in which F_4TCNQ anions intercalated into the P3HT π-stacks.[6] Subsequently, several other studies of F_4TCNQ doping of conjugated polymers also suggested that F_4TCNQ intercalates in the $\pi-\pi$ spacing of P3HT crystallites.[3−5,12,15,16] Inelastic neutron scattering measurements were consistent with a density functional theory (DFT) model based on F_4TCNQ intercalation into the $\pi-\pi$ spacing of P3HT.[12] However, this interpretation is currently questioned with the emergence of sequential doping techniques, which are not sensitive to the phenomena arising from mixed doping (interactions of dopant, host, and solvent prior to film formation).[5] Sequential doping makes use of the ability of small molecular dopants to enter and diffuse in a semicrystalline polymer film. Hence, it allows for regions of well-ordered polymers to form upon film formation, and for one to probe the local structure of the polymer film before contact with, and therefore influence by, the dopant.[13,14,17] Recent studies of P3HT and F_4TCNQ still observe the emergence of a diffraction peak that represents a spacing smaller than the original $\pi-\pi$ distance, regardless of the doping technique: sequential doping from solution[14] or from a dopant vapor.[13,17] However, the observed shape and energetic position of optical P1 polaron absorption are not consistent with strong localization of the P3HT polaron, which would be expected if an F_4TCNQ anion was intercalated between the $\pi-\pi$ stacks of P3HT.[14] The study utilizing vapor doping also suggested that intercalation of dopants between the P3HT backbones is unlikely to occur just from solid-state diffusion.[13] Additionally, experiments in which oriented and highly crystalline P3HT layers were prepared by high-temperature rubbing and subsequent sequential doping from solution corroborate this hypothesis: specifically, the absorption transition dipole of the F_4TNCQ anions was found to be roughly perpendicular to that of the P3HT polaron, which is incompatible with the model of dopants intercalated in the $\pi-\pi$ stacks.[9] Further evidence against the incorporation of dopant molecules into the $\pi-\pi$ stacks as an explanation for different $\pi-\pi$ spacings is given by diffraction measurements of electrochemically doped P3HT: with a continuous increase of $TFSI^-$ anion concentration in a P3HT thin film, the $\pi-\pi$ spacing was found to incrementally decrease—opposed to the formation of a cocrystal with a different but fixed spacing.[8,18] A similar result was found for various dopant ions in different polythiophenes.[19,20] Furthermore, some recent studies on the polymer poly(2,5-bis(3-tetradecylthiophen-2-yl)thieno[3,2-*b*]-thiophene) (PBTTT), which also exhibits the $\pi-\pi$ stacking, revealed a decrease of the $\pi-\pi$ spacing upon doping with various dopants and doping techniques.[9,21−23] This effect was reversed upon dedoping the polymer films.[22,23] Importantly, the change in $\pi-\pi$ spacing was not observed with the structurally similar small-molecule TCNQ, which does not electrically dope PBTTT, implying that the doping process itself is required for the observed reduction of the $\pi-\pi$ spacing.[21]

For doped P3HT, some studies briefly address alternative explanations to an intercalation of dopants in the $\pi-\pi$ stacking as a reason for a change in the stacking distance.[14,17−19] It has been suggested that a change in the side-chain geometry and orientation could influence the distance between π-orbitals on adjacent thiophene rings.[13,14,24] In the case of F_4TNCQ, a specific intercalation in the side chains with an orientation of the long molecular axis perpendicular to the P3HT backbone was proposed.[13] This would lead to a phase change manifesting in the appearance of an additional diffraction peak, which fits to X-ray diffraction measurements.[6,13,14] An observed registry shift of thiophene units on neighboring backbones supports the hypothesis of an altered crystal structure.[14] However, the development of a new crystal phase as a sole reason for a change in the $\pi-\pi$ spacing is ruled out by the observations of a similar stacking distance change in electrochemically doped P3HT.[18] The proposed explanation is still limited to geometrical arguments: straightening of alkyl side chains when the dopant enters the region between the side chains of two adjacent lamellae.[18] This flattening and the additional space that is occupied by the dopant ions would lead to an increase in lamellar spacing—which is observed—and could additionally allow the polymer backbones to stack closer in the $\pi-\pi$ stacking direction.[18] Furthermore, it was suggested that the decreased dihedral angle between neighboring thiophene units upon doping might allow for a denser packing in $\pi-\pi$ stacking direction.[17,19] A more general mechanism that could lead to a change in $\pi-\pi$ spacing upon doping was previously proposed, but not discussed in detail from a theoretical perspective: the delocalization of the polaron across multiple adjacent P3HT backbones, which could slightly pull together the backbones in the $\pi-\pi$ stacking direction.[14]

The studies described above illustrate clearly that the nature of doping and therefore the structure are sensitive to the doping process; therefore, care must be taken in drawing universal conclusions about the structure and properties of conjugated polymers doped with F_4TCNQ when comparing work done by different groups, in different ways, and studied by different techniques. To help develop a self-consistent picture of the doping process, we conducted electron diffraction measurements of P3HT doped with two dopants—F_4TCNQ and molybdenum tris[1-(methoxycarbonyl)-2-(trifluoromethyl)-ethane-1,2-dithiolene] ($Mo(tfd\text{-}CO_2Me)_3$)—with considerably different sizes and shapes, processed by both mixed and sequential doping techniques, in order to probe both the role of the dopant and the processes of doping to determine if any general trends emerged. Specifically, in this work, we provide experimental evidence that does not support intercalation of the dopant anion in the $\pi-\pi$ stacks and we provide a theoretical foundation based on DFT calculations for a mechanism to explain the decreased $\pi-\pi$ stacking distances based on simple molecular orbital (MO) arguments. Our theoretical discussion expands the current discussion from a mostly geometric argumentation to a more general picture that includes the energetics and occupation of intermolecular orbitals upon doping a polymer crystallite. Using DFT, we find that already the removal of electrons from a P3HT crystallite without the physical presence of dopant ions or molecules results in a decrease in $\pi-\pi$ spacing, which is comparable in magnitude to the measured changes in doped thin films. The proposed mechanism is broadly applicable to semiconducting polymers that exhibit $\pi-\pi$ stacking and explains previous observations on PBTTT.[21−23]

DOI: 10.1021/acs.jpcc.8b10845
J. Phys. Chem. C XXXX, XXX, XXX−XXX

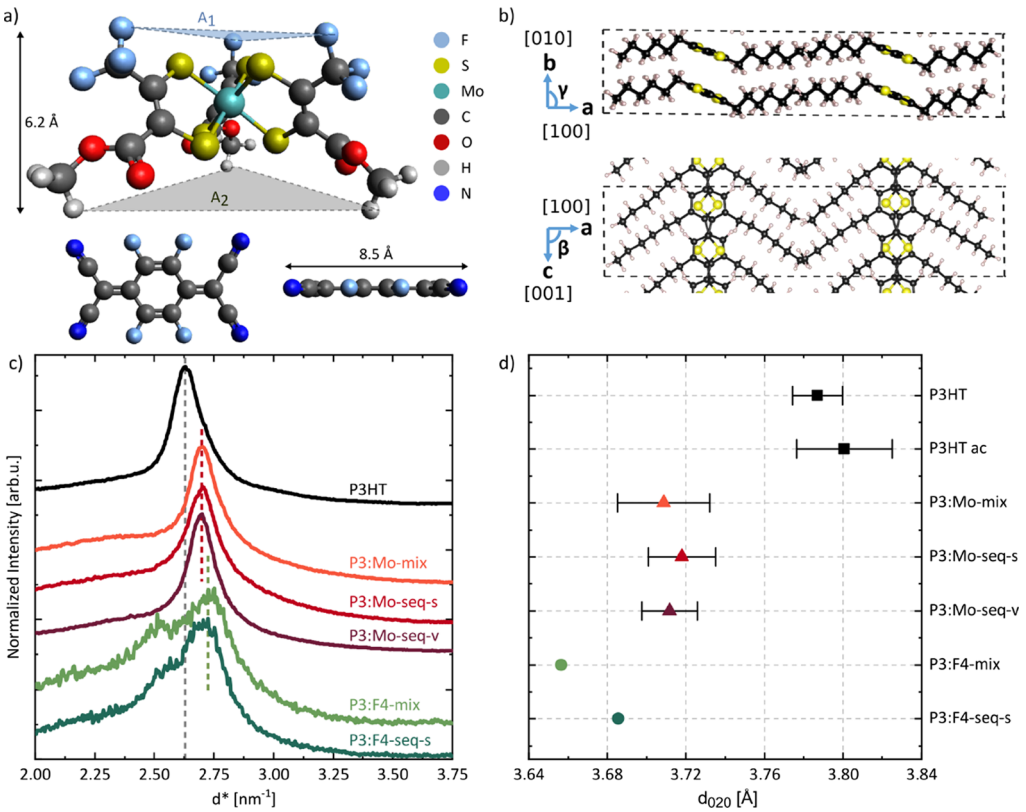

Figure 1. (a) Three-dimensional molecular structures of Mo(tfd-CO_2Me)$_3$ (top) and F_4TCNQ (bottom) with characteristic length dimensions. (b) Crystal structure of P3HT with important stacking directions. (c) Normalized radial profiles of electron diffraction patterns of (liquid nitrogen-cooled) doped and undoped P3HT thin films. The profiles are offset in the *y*-direction for clarity. (d) d_{020} spacing extracted from electron diffraction measurements as shown in (c). The error bars represent the statistical errors from various measurement spots and samples. Error bars are not given for P3:F4 because of the influence of electron dosage on the peak shape and position (see main text for details). P3:P3HT, P3HT ac: P3HT film rinsed with acetonitrile, F4:F_4TCNQ, Mo:Mo(tfd-CO_2Me)$_3$, mix: host and dopant solutions are mixed prior to spin coating, seq-s: sequential doping from acetonitrile solution, seq-v: sequential doping via thermal evaporation of the dopant in vacuum conditions.

2. METHODS

2.1. Materials and Samples Preparation. P3HT (M_w = 31 kg/mol, regioregularity >93%) from Merck and F_4TCNQ (Ossila) were used as received without further purification. Mo(tfd-CO_2Me)$_3$ was synthesized and purified as previously described.[25] For transmission electron microscopy (TEM) electron diffraction measurements, doped and undoped P3HT layers were spin cast on indium tin oxide glass covered with poly(3,4-ethylenedioxythiophene):poly(styrenesulfonate) (PEDOT:PSS). PEDOT:PSS was processed as follows: spin coating at 1000 rpm with 4300 rpm/s for 10 s followed by 4300 rpm with 4300 rpm/s for 30 s and thermal annealing at 140 °C for 30 min. The doped and undoped polymer layers were processed under an inert N_2 atmosphere. After spin coating the polymer layer, deionized water was used to dissolve PEDOT:PSS and float the films off the glass substrates. Hereafter, we skimmed the films with a copper grid (200 mesh) coated with a holey carbon film QUANTIFOIL (3.5/1). For mixed doping, P3HT and the dopants were separately dissolved and stirred for 15 h prior to mixing. The blend solutions were shortly stirred prior to spin coating. We used anhydrous chlorobenzene as the solvent for P3HT and the blends and prepared all solutions at 50 °C under an inert N_2 atmosphere. Film thicknesses were about 50 nm. For sequential doping from solution, 50 nm pristine P3HT was spin coated from chlorobenzene. Subsequently, the dopant was spin coated from acetonitrile. We followed the recipe of Jacobs et al. with a waiting time of 5 s prior to spin coating.[4] For sequential doping of Mo(tfd-CO_2Me)$_3$ via thermal evaporation, layers of pristine P3HT were transferred to ultrahigh vacuum and subsequently the dopant molecule was evaporated with 2.6 Å/min onto P3HT.

2.2. TEM Measurements. Electron diffraction was performed with a Libra 200 MC Kronos, Carl Zeiss Microscopy, at 60 keV acceleration voltage. A total electron dose of ~1850 $e^-/nm^2/s$ was applied for diffraction measurements. The exposure time for the shown measurements on P3HT:F_4TNCQ was 200 ms, whereas the diffraction patterns of P3HT and P3HT:Mo(tfd-CO_2Me)$_3$ were recorded with 1000 ms exposure time. Prior to measurements, the samples were cooled with liquid nitrogen to minimize the beam damage.

2.3. DFT Calculations. *2.3.1. Bulk Geometry.* The bulk geometry is calculated with the VASP code[26,27] The Perdew−Burke−Ernzerhof (PBE) functional[28] and the projector-augmented wave[29,30] methods were applied to treat the electron−electron interaction and the valence−core interaction, respectively. In addition, the empirical D3 dispersion correction[31,32] term was added. A kinetic energy cutoff of 400 eV was selected for the plane wave basis set. The Brillouin zone was sampled using a 1 × 4 × 4 Monkhorst−Pack *k*-point scheme. The total energy convergence criterion was 10^{-4} eV. The system was fully relaxed until the residual Hellmann−Feynman forces were smaller than 0.01 eV/Å.

DOI: 10.1021/acs.jpcc.8b10845
J. Phys. Chem. C XXXX, XXX, XXX−XXX

2.3.2Model Systems with Side Chains. The initial structures of the model systems, dimers of P3HT chains with 5 units (5u) and 10 units (10u), were extracted from the computed P3HT crystal structure (see above). The ground-state geometries of both dimers, the cation-state geometry of the 5u dimer, and the dication-state geometry of the 10u dimer were optimized at the B3-LYP[33−36]/def-SV(P)[37]+D3,[31] level respectively. We fitted two parallel planes for the two chain molecules, respectively. For each fitted plane, the root-mean-square error of the distances of thiophene backbone atoms, excluding the H atoms, to the plane was minimized. The computations for the model systems without hexyl side chains were carried out at the B3-LYP/def-TZVP[37]+D3 level of theory.

3. RESULTS AND DISCUSSION

3.1. Electron Diffraction Measurements. Figure 1 summarizes the electron diffraction measurements of doped and undoped P3HT thin films measured in a transmission electron microscope. Radial profiles of P3HT doped with two different dopants and various doping techniques are shown in Figure 1c. The diffraction maximum at 0.38 nm in the undoped film corresponds to the d_{020} stacking period of P3HT, which corresponds to the $\pi-\pi$ spacing. To investigate the impact of the dopants' spatial dimensions on the crystal lattice of P3HT, the geometrically different dopant molecules F_4TCNQ and Mo(tfd-CO_2Me)$_3$ were chosen. We compare the mixed doping technique, in which dissolved dopant and host are mixed prior to spin coating the blend (P3:Mo-mix and P3:F4-mix with a ratio of one dopant molecule per 10 thiophene monomers), and sequential doping techniques. Sequential doping was performed either from acetonitrile solution (P3:Mo-seq-s and P3:F4-seq-s) or by thermal evaporation of the dopant in vacuum conditions (P3:Mo-seq-v).

To minimize the influence of electron beam on the measured structure, all diffraction measurements were performed by cooling the sample with liquid nitrogen. In contrast to previously published electron diffraction measurements of P3HT:F4TNCQ,[4,5,9] which did not fully reproduce the emergence of the double-peak structure that is observed with X-ray diffraction techniques,[6,13,14] we observe the two spacings with minimized exposure time and cooling of the sample with liquid nitrogen. The major peak appears at smaller spacings compared to that of undoped P3HT, as shown by a fit including the broad background originating from amorphous P3HT (Figure S4 in the Supporting Information). The peak corresponding to a larger spacing compared to that in undoped P3HT might be related to an ordered intercalation of F_4TNCQ into the side chains of P3HT, which is very sensitive to the electron beam as shown in a dosage series (Figure S1 in the Supporting Information). In contrast to the electron-beam-sensitive microstructure of P3HT:F_4TCNQ, the crystallites of Mo(tfd-CO_2Me)$_3$-doped P3HT are significantly more stable and the diffraction pattern does not change in appearance for the utilized exposure times and corresponding electron dosages (see Figure S2 in the Supporting Information). Importantly, upon doping P3HT with the larger molecular dopant Mo(tfd-CO_2Me)$_3$, the d_{020} spacing also decreases; this change is independent of the doping technique within experimental error.

Comparison of diffraction measurements with the two different dopant molecules allows one to gain insights into the local structural order of doped P3HT thin films. As illustrated in Figure 1a, F_4TCNQ is a rather small and planar molecule, compared to the bulky Mo(tfd-CO_2Me)$_3$ (height ≈6.2 Å). Based on the spatial dimensions of F_4TCNQ, incorporation of the dopant in the side chains and the successive emergence of a new crystal phase—as previously proposed[13,14]—seem plausible. However, the fact that we observe a comparable change of d_{020} spacing for the significantly larger dopant Mo(tfd-CO_2Me)$_3$ questions a straightening of side chains as the exclusive explanation for the shift of d_{020} spacing and demands a more general mechanism.

3.2. Density Functional Investigation of Attractive $\pi-\pi$ Interactions. It is well-known that the π-stacking distances between radical cations (or anions) are often rather short compared to those in the π-stacks of neutral molecules,[38−41] and this can be explained in terms of the effect of oxidation (or reduction) on the occupation of bonding and antibonding intermolecular orbitals formed through intermolecular π-overlap. Indeed, Scholes et al. have suggested a similar explanation for the contraction in π-stacking of P3HT on p-doping in terms of interchain polaron delocalization.[14] To further investigate whether such orbital occupancy arguments—rather than the geometric and steric effects of dopant molecules present in the lamellar stacking direction—can explain the observed change of $\pi-\pi$ spacing in doped P3HT, we performed DFT investigations of oligomer models for P3HT. As a starting point, we recalculated the bulk structure of P3HT[42] using the PBE functional[28] and the D3 van der Waals dispersion correction[31] within the VASP program package.[26,27] The computed cell parameter along the [010] direction is b = 7.08 Å, translating to a d_{020} spacing of 3.54 Å. This value is slightly smaller than the experimentally observed value of 3.8 Å for pristine P3HT films, which can be attributed to both disorder effects in the real system and a slight overestimation of bonding by the D3 dispersion correction. Using Becke−Johnson damping[32] does not significantly alter this result. The optimized crystal structure was then used to construct various model systems comprising oligomers identical in the structure to short segments of P3HT. Previous studies found an interaction of one dopant molecule with 4 thiophene units in the case of P3HT:F_4TCNQ, which represents the minimum meaningful length for any calculations. On this basis, and to create conditions comparable to the experiments, we considered a π-dimer of two molecules consisting of 5 thiophene units (5u), from which one electron was removed, representing a doping ratio of 1:10, as in the mixed doping samples. Calculations of other systems can be found in Figures S7.

Figure 2 displays the charge population of the positively charged 5u π-dimer system. The calculations reveal that the one positive charge delocalizes on the two conjugated thiophene backbones. For this 5u dimer system, the d_{020} spacing (extracted from a root-mean-square fit of the molecules to two planes, see "Methods" section) reduces from 3.469 Å in its neutral state to 3.413 Å in its cationic state. Similar calculations for a doubly charged π-dimer of molecules consisting of 10 thiophene units (10u) were conducted and the stacking distance reduces from 3.503 Å of its neutral form to 3.459 Å of its dicationic form. Each positive charge delocalizes in a pattern similar to that of a single positive charge on the 5u dimer and occupies approximately 5 thiophene units (Figure 3). Although the calculated stacking distance change of around 0.05 is smaller than the experimentally observed change

DOI: 10.1021/acs.jpcc.8b10845
J. Phys. Chem. C XXXX, XXX, XXX−XXX

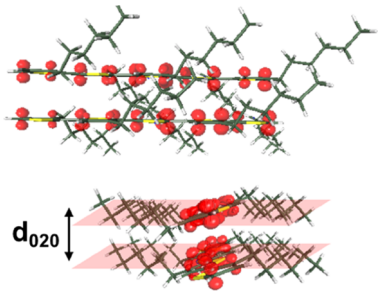

Figure 2. Charge population in a positively charged 5u thiophene dimer model system. The change of d_{020} spacing (Δd_{020}) because of the positive charge is 0.056 Å.

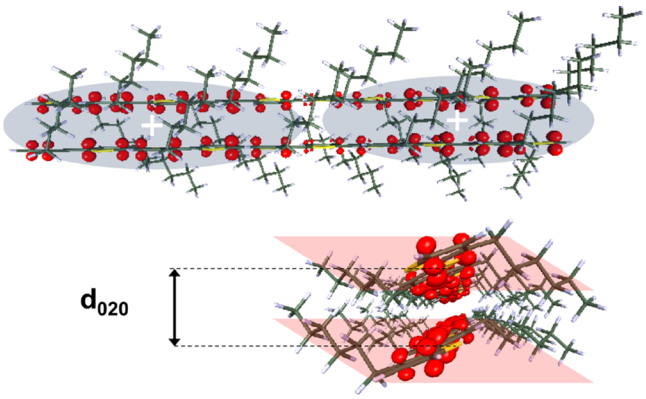

Figure 3. Charge population in a 10u thiophene dimer model system. The decrease of d_{020} spacing (Δd_{020}) because of the positive free charge is 0.044 Å.

between the undoped and doped P3HT thin films ($\Delta d_{P3:Mo}$ = (0.08 ± 0.01) Å, $\Delta d_{P3:F4} \approx 0.12$ Å), it is clearly a significant contribution to the reduction of d_{020}.

The d_{020} spacing is different from but strongly related to the spacing between the π-planes of the thiophene backbones, called d_π in the following. This distance can be extracted from our model by fitting a set of parallel planes to only the thiophene backbones. The angle between the two sets of planes, defining either d_{020} or d_π, is about 27° and the change of the distances should fulfill the simple relation $\Delta d_{020} = \Delta d_\pi \cos(27°)$. In fact, the observed values for Δd_π are larger (0.08 Å for the 5u model and 0.07 Å for 10u) because of an additional horizontal shift of the monomers upon charging.

To track the evolution of $\pi-\pi$ spacing for various sizes of model systems with reasonable computational costs, we carried out further calculations for oligothiophene chains in which the side chains are excluded. One set of calculations starts from the equilibrium P3HT bulk structure, from which dimers (and also trimers and tetramers, see Supporting Information) of π-stacked chains of oligothiophene (with up to 14 thiophene units) have been extracted with the side chains replaced with H atoms. The positions of the replaced H atoms were optimized at the DFT level, whereas the other atoms were kept frozen. In the subsequent computations, the chain geometry was kept fixed and only the $\pi-\pi$ stacking distances (d_π) for the neutral, cationic, and dicationic states were optimized. A second set of calculations employed a slightly different stacking mode for the thiophene chains (see the inset of Figure 4 for a graphical representation).

The computed optimized stacking distances for the neutral, cationic, and dicationic states of the two sets of dimers are plotted in Figure 4. For the cationic states, a strong change of the stacking distance of 0.08 Å relative to the neutral states is found for the shortest chain (4u), which levels off to 0.02 Å for increasing system size. Adding another charge (dicationic states), however, leads to another shortening of the stacking distance, once the chain is long enough to accommodate two charges. This requires 8 units for the P3HT-like stacking pattern and 10 units for the shifted structure. For all chains with more than 10 units, the reduction of d_π in the dicationic state is twice the reduction in the cationic state. In summary, the model calculations confirm the results for the 5u and 10u P3HT model dimer systems discussed above, which show approximately the same shortening of the stacking distance for the singly and doubly charged state, respectively. In addition, although the absolute stacking distance d_π depends on the relative orientation of the two chains, see Figure 4, its reduction upon charging Δd_π is nearly independent of it.

To explain the measured and calculated decrease in $\pi-\pi$ spacing, a closer look at the frontier orbitals, which delocalize on the dimer, is instructive. In Figure 5, we applied MO localization on each thiophene chain monomer. The corresponding MO diagram shows that the highest occupied MO (HOMO) and HOMO − 1 of the dimer system can be considered as, respectively, antibonding and bonding linear combination of two monomer HOMOs. Hence, a positive charge (corresponding to the removal of one electron from the antibonding orbital) weakens the antibonding effect; the $\pi-\pi$

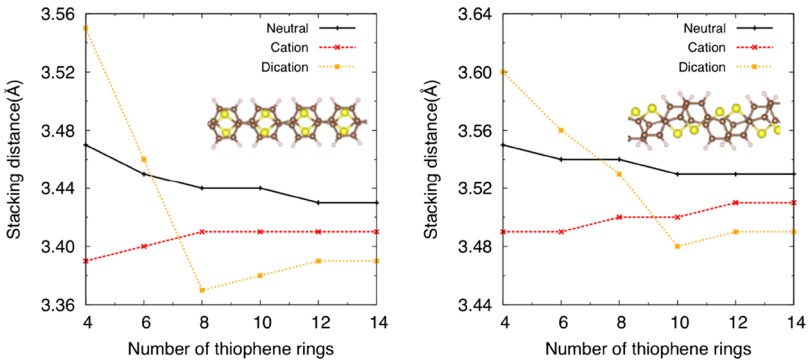

Figure 4. Equilibrium $\pi-\pi$ stacking distance of the two sets of polythiophene dimers at different chain lengths for neutral (black line), cationic (red line), and dicationic (orange line) states, respectively. The left figure uses a model based on the stacking geometry of ideal crystalline P3HT and the right figure is based on an alternative model where one of the chains is shifted along the c direction as shown in the insert.

DOI: 10.1021/acs.jpcc.8b10845
J. Phys. Chem. C XXXX, XXX, XXX−XXX

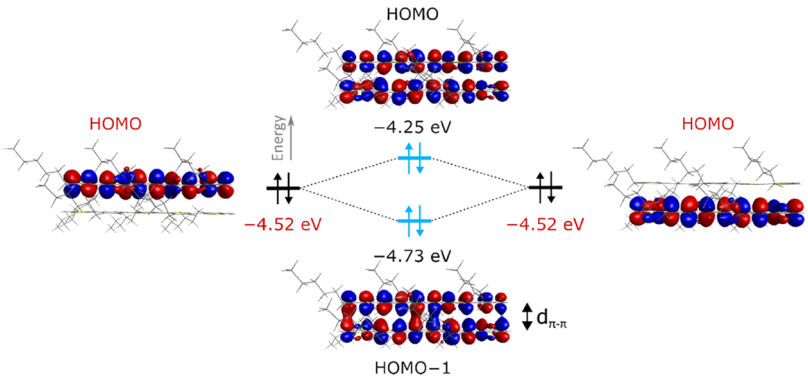

Figure 5. Frontier MO diagram of the 5u model dimer system. The middle column shows the HOMO and HOMO − 1 canonical MOs, whereas the left (right) column shows the degenerate HOMO of the localized MO on the upper (lower) polythiophene backbone.

stacking distance reduces as a direct consequence of the charging, without the physical presence of a dopant molecule. Moreover, our calculations show that a delocalization of the positive charge in the stacked polythiophene chains is energetically more favorable compared to a localization on a single chain (see Supporting Information for a detailed energy decomposition analysis).

Finally, the charge population on a series of large polythiophene oligomers was calculated, see Figure S7. The plot shows that each charge locates on one end of the backbone chain, respectively, and strengthens the $\pi-\pi$ stacking on each end separately. Thus, the following model for the observed structural changes emerges from our calculations: upon doping, for each dopant molecule, 1 unit positive charge is created in the neighboring P3HT crystal domain. The charges localize statistically in the P3HT and lead to attractive forces between the chains and in consequence to a reduced average $\pi-\pi$ stacking distance. Reorganization of the crystal structure due to the incorporation of dopant molecules into the side-chain region, as suggested in refs 9 and 24, may in addition contribute, resulting in the observed reduction of stacking distance of up to 0.1 Å.

4. CONCLUSIONS

In summary, this work is consistent with several recent studies in suggesting that intercalation of dopant molecules into P3HT d_{020} stacking does not universally explain the observed reductions of d_{020} spacing upon doping. Although our diffraction data do not rule out F_4TCNQ intercalation, a comparable reduction of d_{020} spacing on doping with the much larger Mo(tfd-CO_2Me)$_3$ strongly suggests an alternative origin. The reduction in d_{020} spacing seen for both dopants is attributed to the removal of electrons on p-doping from antibonding intermolecular orbitals; DFT calculations for a model dimer give decreases in π-spacing similar to the experimentally observed values. We certainly acknowledge that many factors will impact the final solid-state structure of a semiconducting polymer and the situation will be even more complex for a doped material as is the subject of our paper. These include the simple packing effects to maximize the density, electrostatic interactions, and the effect of the polaron interacting with a nearby chain, which themselves can have purely electrostatic effects as well as those arising from hybridization, which we have highlighted. The ultimate structure will be influenced by all these effects and the observed structure itself may not always even reflect a thermodynamic minimum. An improved understanding of the spatial position of dopant molecules and the origin of changes in the crystal spacing and structure are valuable for the understanding of the underlying processes of molecular doping in terms of charge separation and the corresponding doping efficiency. Furthermore, the previously shown correlation between doping-induced lattice strain and charge carrier mobility in doped P3HT[8,24] illustrates the need for a detailed understanding of the local structural order.

■ ASSOCIATED CONTENT

Supporting Information

The Supporting Information is available free of charge on the ACS Publications website at DOI: 10.1021/acs.jpcc.8b10845.

Electron diffraction dosage series of P3HT:F_4TCNQ and Mo(tfd-CO_2Me)$_3$ as well as a fit to low-dosage electron diffraction profiles of P3HT:F_4TNCQ; DFT bulk structures of P3HT and polythiophene; energy decomposition analysis of a polythiophene trimer system; and DFT calculations of larger model systems without side chains (PDF)

■ AUTHOR INFORMATION

Corresponding Authors

*E-mail: koehn@theochem.uni-stuttgart.de (A.K.).
*E-mail: r.lovrincic@tu-braunschweig.de (R.L.).

ORCID

Lars Müller: 0000-0001-7321-4702
Stephen Barlow: 0000-0001-9059-9974
Seth R. Marder: 0000-0001-6921-2536
Andreas Köhn: 0000-0002-0844-842X
Robert Lovrincic: 0000-0001-5429-5586

Author Contributions

¶W.L. and L.M. contributed equally to this work.

Notes

The authors declare no competing financial interest.

■ ACKNOWLEDGMENTS

The authors acknowledge the German Federal Ministry of Education and Research (BMBF) for financial support within the InterPhase project (FKZ 13N13656 and 13N13663), the Office of Naval Research for support through grant no. N00014-14-1-0126, and the NSFC project no. 21703023. L.M. gratefully acknowledges the scholarship granted by Carl Zeiss Foundation. The authors furthermore greatly appreciate the

synthesis of Mo(tfd-CO_2Me)$_3$ carried out by Yadong Zhang. S.R.M. and S.B. thank the U. S. National Science foundation for support of this work through the DMREF program, under award no. DMR-1729737.

■ REFERENCES

(1) Malliaras, G.; Friend, R. An Organic Electronics Primer. *Phys. Today* **2005**, *58*, 53−58.

(2) Salzmann, I.; Heimel, G. Toward a comprehensive understanding of molecular doping organic semiconductors (review). *J. Electron Spectrosc. Relat. Phenom.* **2015**, *204*, 208−222.

(3) Scholes, D. T.; Hawks, S. A.; Yee, P. Y.; Wu, H.; Lindemuth, J. R.; Tolbert, S. H.; Schwartz, B. J. Overcoming Film Quality Issues for Conjugated Polymers Doped with F_4TCNQ by Solution Sequential Processing: Hall Effect, Structural, and Optical Measurements. *J. Phys. Chem. Lett.* **2015**, *6*, 4786−4793.

(4) Jacobs, I. E.; Aasen, E. W.; Oliveira, J. L.; Fonseca, T. N.; Roehling, J. D.; Li, J.; Zhang, G.; Augustine, M. P.; Mascal, M.; Moulé, A. J. Comparison of Solution-Mixed and Sequentially Processed P3HT:F_4TCNQ Films: Effect of Doping-Induced Aggregation on Film Morphology. *J. Mater. Chem. C* **2016**, *4*, 3454−3466.

(5) Müller, L.; Nanova, D.; Glaser, T.; Beck, S.; Pucci, A.; Kast, A. K.; Schröder, R. R.; Mankel, E.; Pingel, P.; Neher, D.; et al. Charge-Transfer-Solvent Interaction Predefines Doping Efficiency in p-Doped P3HT Films. *Chem. Mater.* **2016**, *28*, 4432−4439.

(6) Duong, D. T.; Wang, C.; Antono, E.; Toney, M. F.; Salleo, A. The Chemical and Structural Origin of Efficient P-Type Doping in P3HT. *Org. Electron.* **2013**, *14*, 1330−1336.

(7) Duong, D. T.; Phan, H.; Hanifi, D.; Jo, P. S.; Nguyen, T.-Q.; Salleo, A. Direct Observation of Doping Sites in Temperature-Controlled, p-Doped P3HT Thin Films by Conducting Atomic Force Microscopy. *Adv. Mater.* **2014**, *26*, 6069−6073.

(8) Thelen, J. L.; Wu, S.-L.; Javier, A. E.; Srinivasan, V.; Balsara, N. P.; Patel, S. N. Relationship between Mobility and Lattice Strain in Electrochemically Doped Poly(3-Hexylthiophene). *ACS Macro Lett.* **2015**, *4*, 1386−1391.

(9) Hamidi-Sakr, A.; Biniek, L.; Bantignies, J.-L.; Maurin, D.; Herrmann, L.; Leclerc, N.; Lévêque, P.; Vijayakumar, V.; Zimmermann, N.; Brinkmann, M. A Versatile Method to Fabricate Highly In-Plane Aligned Conducting Polymer Films with Anisotropic Charge Transport and Thermoelectric Properties: The Key Role of Alkyl Side Chain Layers on the Doping Mechanism. *Adv. Funct. Mater.* **2017**, *27*, 1700173.

(10) Ihn, K. J.; Moulton, J.; Smith, P. Whiskers of poly(3-alkylthiophene)s. *J. Polym. Sci., Part B: Polym. Phys.* **1993**, *31*, 735−742.

(11) Merlo, J. A.; Frisbie, C. D. Field Effect Transport and Trapping in Regioregular Polythiophene Nanofibers. *J. Phys. Chem. B* **2004**, *108*, 19169−19179.

(12) Harrelson, T. F.; Cheng, Y. Q.; Li, J.; Jacobs, I. E.; Ramirez-Cuesta, A. J.; Faller, R.; Moulé, A. J. Identifying Atomic Scale Structure in Undoped/Doped Semicrystalline P3HT Using Inelastic Neutron Scattering. *Macromolecules* **2017**, *50*, 2424−2435.

(13) Lim, E.; Peterson, K. A.; Su, G. M.; Chabinyc, M. L. Thermoelectric Properties of Poly(3-hexylthiophene) (P3HT) Doped with 2,3,5,6-Tetrafluoro-7,7,8,8-tetracyanoquinodimethane (F4TCNQ) by Vapor-Phase Infiltration. *Chem. Mater.* **2018**, *30*, 998−1010.

(14) Scholes, D. T.; Yee, P. Y.; Lindemuth, J. R.; Kang, H.; Onorato, J.; Ghosh, R.; Luscombe, C. K.; Spano, F. C.; Tolbert, S. H.; Schwartz, B. J. The Effects of Crystallinity on Charge Transport and the Structure of Sequentially Processed F_4TCNQ-Doped Conjugated Polymer Films. *Adv. Funct. Mater.* **2017**, *27*, 1702654.

(15) Wang, C.; Duong, D. T.; Vandewal, K.; Rivnay, J.; Salleo, A. Optical Measurement of Doping Efficiency in Poly(3-Hexylthiophene) Solutions and Thin Films. *Phys. Rev. B: Condens. Matter Mater. Phys.* **2015**, *91*, 085205.

(16) Méndez, H.; Heimel, G.; Winkler, S.; Frisch, J.; Opitz, A.; Sauer, K.; Wegner, B.; Oehzelt, M.; Röthel, C.; Duhm, S.; et al. Charge-Transfer Crystallites as Molecular Electrical Dopants. *Nat. Commun.* **2015**, *6*, 8560.

(17) Hynynen, J.; Kiefer, D.; Yu, L.; Kroon, R.; Munir, R.; Amassian, A.; Kemerink, M.; Müller, C. Enhanced Electrical Conductivity of Molecularly P-Doped Poly(3-Hexylthiophene) through Understanding the Correlation with Solid-State Order. *Macromolecules* **2017**, *50*, 8140−8148.

(18) Guardado, J. O.; Salleo, A. Structural Effects of Gating Poly(3-Hexylthiophene) through an Ionic Liquid. *Adv. Funct. Mater.* **2017**, *27*, 1701791.

(19) Kawai, T.; Nakazono, M.; Yoshino, K. Effects of Doping on the Crystal Structure of Poly(3-Alkylthiophene). *J. Mater. Chem.* **1992**, *2*, 903−906.

(20) Tashiro, K.; Kobayashi, M.; Kawai, T.; Yoshino, K. Crystal structural change in poly(3-alkyl thiophene)s induced by iodine doping as studied by an organized combination of X-ray diffraction, infrared/Raman spectroscopy and computer simulation techniques. *Polymer* **1997**, *38*, 2867−2879.

(21) Cochran, J. E.; Junk, M. J. N.; Glaudell, A. M.; Miller, P. L.; Cowart, J. S.; Toney, M. F.; Hawker, C. J.; Chmelka, B. F.; Chabinyc, M. L. Molecular Interactions and Ordering in Electrically Doped Polymers: Blends of PBTTT and F_4TCNQ. *Macromolecules* **2014**, *47*, 6836−6846.

(22) Patel, S. N.; Glaudell, A. M.; Kiefer, D.; Chabinyc, M. L. Increasing the Thermoelectric Power Factor of a Semiconducting Polymer by Doping from the Vapor Phase. *ACS Macro Lett.* **2016**, *5*, 268−272.

(23) Patel, S. N.; Glaudell, A. M.; Peterson, K. A.; Thomas, E. M.; O'Hara, K. A.; Lim, E.; Chabinyc, M. L. Morphology Controls the Thermoelectric Power Factor of a Doped Semiconducting Polymer. *Sci. Adv.* **2017**, *3*, No. e1700434.

(24) Thomas, E. M.; Brady, M. A.; Nakayama, H.; Popere, B. C.; Segalman, R. A.; Chabinyc, M. L. X-Ray Scattering Reveals Ion-Induced Microstructural Changes During Electrochemical Gating of Poly(3-Hexylthiophene). *Adv. Funct. Mater.* **2018**, *28*, 1803687.

(25) Dai, A.; Zhou, Y.; Shu, A. L.; Mohapatra, S. K.; Wang, H.; Fuentes-Hernandez, C.; Zhang, Y.; Barlow, S.; Loo, Y.-L.; Marder, S. R.; et al. Enhanced Charge-Carrier Injection and Collection via Lamination of Doped Polymer Layers p-Doped with a Solution-Processible Molybdenum Complex. *Adv. Funct. Mater.* **2014**, *24*, 2197−2204.

(26) Kresse, G.; Furthmüller, J. Efficient iterative schemes for ab initio total-energy calculations using a plane-wave basis set. *Phys. Rev. B: Condens. Matter Mater. Phys.* **1996**, *54*, 11169−11186.

(27) Kresse, G.; Furthmüller, J. Efficiency of Ab-Initio Total Energy Calculations for Metals and Semiconductors Using a Plane-Wave Basis Set. *Comput. Mater. Sci.* **1996**, *6*, 15−50.

(28) Perdew, J. P.; Burke, K.; Ernzerhof, M. Generalized Gradient Approximation Made Simple. *Phys. Rev. Lett.* **1996**, *77*, 3865−3868.

(29) Blöchl, P. E. Projector Augmented-Wave Method. *Phys. Rev. B: Condens. Matter Mater. Phys.* **1994**, *50*, 17953−17979.

(30) Kresse, G.; Joubert, D. From Ultrasoft Pseudopotentials to the Projector Augmented-Wave Method. *Phys. Rev. B: Condens. Matter Mater. Phys.* **1999**, *59*, 1758−1775.

(31) Grimme, S.; Antony, J.; Ehrlich, S.; Krieg, H. A Consistent and Accurate Ab Initio Parametrization of Density Functional Dispersion Correction (DFT-D) for the 94 Elements H-Pu. *J. Chem. Phys.* **2010**, *132*, 154104.

(32) Grimme, S.; Ehrlich, S.; Goerigk, L. Effect of the Damping Function in Dispersion Corrected Density Functional Theory. *J. Comput. Chem.* **2011**, *32*, 1456−1465.

(33) Becke, A. D. Density-functional thermochemistry. III. The role of exact exchange. *J. Chem. Phys.* **1993**, *98*, 5648−5652.

(34) Lee, C.; Yang, W.; Parr, R. G. Development of the Colle-Salvetti Correlation-Energy Formula into a Functional of the Electron Density. *Phys. Rev. B: Condens. Matter Mater. Phys.* **1988**, *37*, 785−789.

DOI: 10.1021/acs.jpcc.8b10845
J. Phys. Chem. C XXXX, XXX, XXX−XXX

(35) Vosko, S. H.; Wilk, L.; Nusair, M. Accurate Spin-Dependent Electron Liquid Correlation Energies for Local Spin Density Calculations: A Critical Analysis. *Can. J. Phys.* **1980**, *58*, 1200−1211.
(36) Stephens, P. J.; Devlin, F. J.; Chabalowski, C. F.; Frisch, M. J. Ab Initio Calculation of Vibrational Absorption and Circular Dichroism Spectra Using Density Functional Force Fields. *J. Phys. Chem.* **1994**, *98*, 11623−11627.
(37) Schäfer, A.; Horn, H.; Ahlrichs, R. Fully Optimized Contracted Gaussian Basis Sets for Atoms Li to Kr. *J. Chem. Phys.* **1992**, *97*, 2571−2577.
(38) Nishinaga, T.; Komatsu, K. Persistent π Radical Cations: Self-Association and Its Steric Control in the Condensed Phase. *Org. Biomol. Chem.* **2005**, *3*, 561−569.
(39) Okajima, H.; Shinmyozu, T.; Sakamoto, A. Selective resonance Raman enhancement of large amplitude inter-ring vibrations of [34](1,2,4,5)cyclophane radical cation; a model of π-stacked dimer radical ions. *Phys. Chem. Chem. Phys.* **2018**, *20*, 3395−3402.
(40) Yamazaki, D.; Nishinaga, T.; Tanino, N.; Komatsu, K. Terthiophene Radical Cations End-Capped by Bicyclo[2.2.2]octene Units: Formation of Bent π-Dimers Mutually Attracted at the Central Position. *J. Am. Chem. Soc.* **2006**, *128*, 14470−14471.
(41) Lü, J.-M.; Rosokha, S. V.; Kochi, J. K. Stable (Long-Bonded) Dimers via the Quantitative Self-Association of Different Cationic, Anionic, and Uncharged π-Radicals: Structures, Energetics, and Optical Transitions. *J. Am. Chem. Soc.* **2003**, *125*, 12161−12171.
(42) Dag, S.; Wang, L.-W. Packing Structure of Poly(3-Hexylthiophene) Crystal: Ab Initio and Molecular Dynamics Studies. *J. Phys. Chem. B* **2010**, *114*, 5997−6000.

DOI: 10.1021/acs.jpcc.8b10845
J. Phys. Chem. C XXXX, XXX, XXX−XXX